



# Determination of the forming limit of impact hydroforming by frictionless full zone hydraulic forming test

Yan Ma<sup>1</sup> · Shuai-feng Chen<sup>1</sup> · Da-yong Chen<sup>1</sup> · Dorel Banabic<sup>2</sup> · Hong-wu Song<sup>1</sup> · Yong Xu<sup>1</sup> · Shi-hong Zhang<sup>1</sup> · Xiao-shuai Fan<sup>3</sup> · Qiang Wang<sup>3</sup>

Received: 4 December 2020 / Accepted: 1 July 2021 / Published online: 19 July 2021

© The Author(s), under exclusive licence to Springer-Verlag France SAS, part of Springer Nature 2021

## Abstract

It is impossible to obtain the forming limit curve (FLC) by full zone hydraulic forming test under quasi-static (QS) condition since the liquid will leak from the notches of the specimen once the pressure increases. In this study, a novel method is proposed to investigate the frictionless full zone hydraulic FLC of AA5A06 under high strain rate (HSR) condition based on the impact hydroforming technology (IHF). It is found that the FLC is increased significantly by IHF compared with the quasi-static rigid punch (QS-R) forming and the quasi-static hydraulic (QS-H) forming. Differentiating with the QS-H, the increase amounts of FLC at the biaxial tension zone and the tension-compression zone are notably different for IHF. Additionally, the theoretical calculations of FLC is conducted by using M-K model combining with Hill48 anisotropic yield criterion under QS and HSR conditions. The results calculated by the M-K model reasonably agree with the ones obtained from experimentation under QS and HSR condition, and a higher initial thickness ratio is assigned for HSR considering the neck postponing effect of inertia.

**Keywords** forming limit curve · impact hydroforming · high strain rate · frictionless

## Introduction

Hydroforming (HF) has attracted much attention as an advanced lightweight forming technology, due to its irreplaceable advantages in producing complex shaped components [1]. In addition, HF is able to increase the forming limit compared with the press forming [2], therefore many researchers studied the hydraulic forming limit curve (FLC) [3]. However, the test was mostly used to obtain the equal-biaxial result with the whole sheet because of the sealing requirement [4]. It can be extended to the whole biaxial zone of the FLC by changing the eccentricity of the oval shape die cavity [5]. Several methods were considered to realize the test of the tension-compression zone of the FLC, afterwards they can

expand the hydraulic FLC to the whole zone. One of the methods is to adopt the carrier sheet to seal the liquid, then the specimen can deform with the carrier sheet. Banabic et al. [6] used low carbon steel sheet as the carrier sheet, Chen et al. [7] used the Polyurethane plate. But the friction was introduced by this method between the carrier sheet and the specimens which has remarkable effect to the FLC [8]. Therefore, it is impossible to get frictionless full zone hydraulic FLC under quasi-static (QS) condition. This issue was solved by using the impact hydroforming (IHF) because of the advantages of high strain rate [9], and the frictionless full zone hydraulic FLC was first time realized. Compared with the IHF condition for AA5A06, the quasi-static rigid punch condition and quasi-static hydraulic condition were named as QS-R and QS-H, respectively.

Many researchers in the metal forming field investigated the hydraulic bulge formability of sheet under different strain rate for the biaxial zone. Broomhead and Grieve [10] are the first scholars who use hydraulic bulge test to investigate the influence of strain rate on the strain to fracture of sheet metals under biaxial condition. As a result, FLC of low carbon steel was determined successfully at strain rates of up to  $70 \text{ s}^{-1}$ , in which increasing strain rate leads to lowering the FLC. Grolleau et al. [5] performed a dynamic bulge tests on 6111-T4 Al alloy sheets under

✉ Yan Ma  
yma@imr.ac.cn

<sup>1</sup> Institute of Metal Research (IMR), Chinese Academy of Sciences (CAS), Shenyang 110016, China

<sup>2</sup> Department of Manufacturing Engineering, Technical University of Cluj-Napoca, 400641 Cluj-Napoca, Romania

<sup>3</sup> School of Mechanical Engineering, University of Jinan, 250022 Jinan, China

equi-biaxial condition by using Split Hopkinson Pressure Bar (SHPB) with a water cell and viscoelastic nylon bars, and the equivalent plastic strain rate is about  $300 \text{ s}^{-1}$ . They calculated the equivalent strain of aluminum 6111-T4 sheets based on the strain signals, and suggested that the stress strain curves obtained from dynamic bulge tests are more reliable than the ones from conventional tension tests. Ramezani and Ripin [11] further optimized this method by changing the fluid to rubber. It can be concluded that the strain of the AA6005-T6 increased under equi-biaxial condition with the increasing of strain rate (impact velocity). Justusson et al. [12] investigated the response of multi-axial strain of thin 3003 Al-Mn sheet under strain rate range of  $200\text{--}850 \text{ s}^{-1}$  by developing a shock tube setup. The alloy shows remarkable ductility and plasticity at high strain rates. There are also researches concerned about high strain rate (HSR) formability by electromagnetic forming and electro-hydraulic forming. Golovashchenko [13] found that the formability of AA6111-T4 can be improved by electromagnetic forming, and a driven sheet is needed for the non-magnetic test material. Yu et al. [14] found a relative increase of 17.5–70 % in major strain obtained by electro-hydraulic forming relative to that obtained by quasi-static forming, but the electro-hydraulic forming limit experiment still need a carrier sheet.

This paper also investigated if the traditional FLC calculation theory is able to predict the HSR FLC accurately. The HSR FLC experiments are very complicated, if the traditional FLC calculation theories are valid to HSR condition, the FLC under HSR condition can be set up just according to the results of some easier HSR tensile tests, and the result will be a highly efficient guide to estimate whether a part can be formed successfully or not under the IHF by simulation. Verleysen et al. [15] investigated the theoretical prediction of the FLC by M-K model to 4 kinds of steels under QS and HSR ( $1000 \text{ s}^{-1}$ ) conditions. The hardening models are Johnson–Cook (JC) model and the Voce model, and the calculation adopted the isotropic yield criterion. It is found that the HSR FLCs of S235 and DC04 are significantly lower than the static ones. The FLCs of QS and HSR condition of AISI 409 are almost coincide. But the HSR FLC of CMnAl TRIP is higher than the QS one. The HSR FLC is theoretically calculated by M-K theory in this study. The plastic anisotropy was also taken into account during the calculation by introducing the anisotropy yield criterion, this was seldom discussed in the dynamic field.

## Experimental procedure

### Investigated material

The thickness of AA5A06-O sheet is 1 mm in the study. The chemical compositions and microstructure of AA5A06 before testing were depicted in Table 1; Fig. 1, respectively.

## FLC experiment setup

### Quasi-static FLC experiment setup

The QS-R bulge test was conducted according to the ISO 12004-2 standard. Experiments were implemented by the commercial sheet metal forming testing machine BCS-50BR. The diameter of the punch is 100 mm. The diameter of the specimens for the QS-R bulge experiments is 180 mm. There are two circle notches at the outside with 180 mm diameter. And the inner distance of two notches varied from 20 mm to 180 mm with 20 mm interval. A series of 2.5 mm diameter circles were etched on the sheet by using an electro-chemical method before testing, which were used to calculate the strain. In the whole forming procedure, the grids were deformed and their circular shapes changed into ellipses with the minor and major axes characterizing the direction of principal strains. The values of these principal strains at failure can be acquired through calculating the minor and major axes of the ellipses close to the fracture site and matching them with the initial diameter of the grids.

The QS-H bulge test employed Banabic method [6] to reduce the friction effect to the FLC by considering that the friction coefficient of steel-aluminum (0.15) is lower than that of the Polyurethane-aluminum (0.25) [16]. The configuration used under QS-H condition was a conventional set-up for the bulge test as shown in Fig. 2(a). Two layers sheets were fixed between the die and the blank holder. The upper blank has a pair of holes pierced in symmetric positions with respect to the center, while the lower blank acts both as a carrier and a deformable punch. The clamping force between the die and the blank holder should be large enough to avoid sheets sliding between the dies by the hydraulic press. Through the test, the unclamped part of the specimens is forced to deform into the shape of hemisphere by the deformation of the carrier sheet under constantly growing the pressure of the fluid. The bulged upper sheet will crack just after the deformation of the material exceeds its forming limit.

The dimensions of the specimens for the QS-H bulge experiments are shown in Fig. 2(b). The diameter of the specimens is 150 mm. There are two holes, the inner distance  $D$  of the two holes varied from 20 mm to 80 mm with the interval 10 mm. There are eight kinds of specimens in total including the whole sheet specimen. The radius  $R$  of the fillets is 10 mm, 5mm, 3mm when  $D$  is in the range of 20 mm to 50 mm, 60 mm and 70 mm, 80 mm, respectively. The carrier sheet is low carbon steel.

### Experiment setup for FLC of impact hydroforming

The IHF FLC test setup is depicted in Fig. 3. The projectile flew at high speed after firing out by the high pressure of the light gas gun. Afterwards, the projectile impacted on the

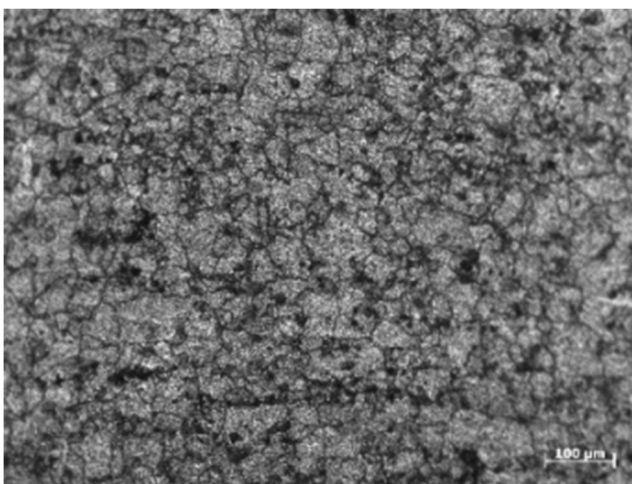
**Table 1** Chemical compositions of AA5A06 detected by OES

Element	Mg	Mn	Fe	Si	Ti	Zn	Cu	Be
Percent	6.50	0.54	0.16	0.06	0.06	< 0.05	< 0.05	0.0005

piston which sealed the water chamber. The high pressure of water was produced by the impact of the projectile and piston together, and the sheet deformed under this high pressure. This testing system can get different strain rates by adjusting the firing pressure of light gas gun. The projectile was steel plate with plastic seat behind it. The weight of the projectile and the piston are 1862.6 and 902.4 g respectively. The setup must be laid vertically. The polyvinylidene fluoride (PVDF) film transducer was used to detect the forming time and shock wave pressure at the interface between water and sheet [17]. The PVDF is flexible so it can deform with the sheet, and the pulse signals of shock wave produced by PVDF were captured by the oscilloscope. The shock wave pulse duration is treated as the deformation time in this study.

The dimensions of specimens of IHF FLC experiments are shown in Fig. 4. The out diameter is 114 mm. There are 9 kinds of specimens in total, and the detailed dimensions of parameters A, B, C and R are listed in Table 2. The impact velocities of specimens No. 1–9 are also listed in Table 2. There is a lot of energy loss at the notch location of the specimen, therefore the impact velocities for the tensile-compression zone specimens are higher than that for the biaxial zone specimens. The geometry of the specimen will affect the strain rate, in order to get a similar strain rate for all the specimens, the narrower the specimen the higher the impact velocity. It is found that the strain rate will decrease with the decrease of the width of the specimen under the same impact velocity.

During QS-H experiment, the liquid will flow out from the specimen notches (Fig. 5a) when increasing the pressure if

**Fig. 1** Microstructure of 5A06-O sheet

there are not carrier sheet below the specimens to seal the liquid, then the specimens cannot be deformed. Due to the very high impact velocity of IHF, the dynamic pressure of the water is a shock wave pulse which is different from Pascal pressure principle under the QS condition. Afterwards, the specimens deformed or cracked in tens of microseconds (Fig. 5b), therefore the tension-compression zone of the FLC is able to be achieved.

### FLC of QS and IHF experiments

The same material, isotropic or anisotropic, must have different forming limits. Regardless of the sampling direction of the forming limit sample, it will be affected by anisotropy. In order to ensure that the anisotropy has the same effect on all specimens, the forming limit specimens in this study are all taken in the rolling direction. The FLC of QS-R, QS-H and IHF conditions are shown in the Fig. 6. In order to reduce the artificial error of manually point selection the author selected multiple points in each sample instead of one point to plot the FLC curves. In other words, some points are selected at a given specimen, and then all the related major/minor strains are plotted to obtain the FLC. The experiment results get from the measurement is  $\varepsilon_{11}$ ,  $\varepsilon_{22}$ ,  $\varepsilon_{33}$ , already take into account the orthotropy. Then, the major strain  $\varepsilon_1$  and minor strain  $\varepsilon_2$  are calculated with the software linked to the experimental mesh system. It is found that the IHF is able to realize the test of the tension-compression zone of FLC without carrier sheet, and the frictionless full zone hydraulic FLC is successfully achieved. The IHF FLC enlarges both the range of major and minor strain range compared with the QS conditions. The quantity analysis is performed for the biaxial tension zone, tension-compression zone and the full zone. For the biaxial tension zone, the IHF increase the range of the minor strain by 772.19 and 38.32 % compared with QS-R and QS-H respectively. Moreover, IHF increases the range of the major strain by 136.16 and 74.22 % compared with QS-R and QS-H respectively. For the tension-compression zone, the IHF increases the range of the minor strain by 48.82 and 32.27 % compared with QS-R and QS-H respectively. Meanwhile IHF increases the range of the major strain by 48.82 and 33.27 % compared with QS-R and QS-H respectively. For the whole FLC zone, the IHF increases the range of the minor strain by 210.47 and 36.39 % compared with QS-R and QS-H respectively.

The study of Maris [18] found that the HSR FLC of 5182-O equally increased compared with the QS FLC for the whole

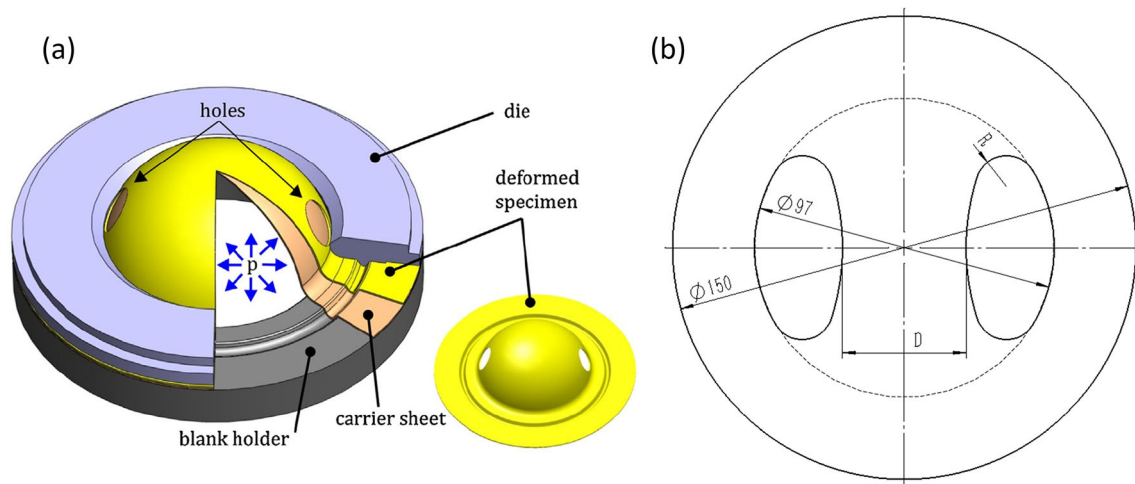


**Fig. 2** (a) The schematic of the QS-H FLC experimental (b) Specimens of QS-H

zone. This study found that the increase between the FLCs of IHF and QS-H for the biaxial tension zone and tension-compression zone are different. The distance between the two lines are 0.066 and 0.02313 for the biaxial tension zone and tension-compression zone respectively.

Three main classical strain ratios (uniaxial ( $\beta = -1/2$ ), plane stress ( $\beta = 0$ ), equal biaxial ( $\beta = 1$ )) and other seven strain ratios were selected to compare the three kinds of FLC. The maximum increases of effective strain for the IHF FLC are located at  $\beta = \pm 1/3$  compared with QS-R, both exceeds 80%. The maximum increases of effective strain for the IHF FLC are located at  $\beta = -1/3$  and  $\beta = 1/3 \sim 1$  compared with QS-H, both exceeds 40%. It is also found that QS-R is difficult to get the biaxial strain due to the crack position is far away from the center of the specimens.

The maximum effective strains are 0.264, 0.341 and 0.468 for QS-R, QS-H and IHF FLC respectively. The forming time of QS test is about 60 s. The pressure wave acting on the IHF FLC experiment specimens are depicted in Fig. 7, the forming time of IHF test is about 102–150  $\mu\text{s}$ , taking 200  $\mu\text{s}$  as the

forming time by considering there are measurement errors. The strain rates are  $4.4 \times 10^{-3} \text{ s}^{-1}$ ,  $5.7 \times 10^{-3} \text{ s}^{-1}$  and  $2.43 \times 10^3 \text{ s}^{-1}$  for QS-R, QS-H and IHF FLC respectively.

### Tensile test under QS and HSR conditions

For the QS condition, the stress strain curves were obtained by the 100 kN Instron 5980 tensile machine. The dimensions of the QS tensile specimens are depicted in Fig. 8 according to Chinese Standard GB/T 228.2–2015, gauge length is 20mm.

The HSR tensile tests were accomplished by Split Hopkinson Tensile Bar (SHTB). The anisotropy of the material is considered both in the quasi-static tensile test and Hopkinson test by adopting the specimens of rolling,  $45^\circ$  and transverse directions. The schematic of SHTB [19] is depicted as Fig. 9. The tensile specimen is clamped between incident bar and transmitted bar with a diameter of 20 mm. The incident bar is impacted by a striker tube with high speed

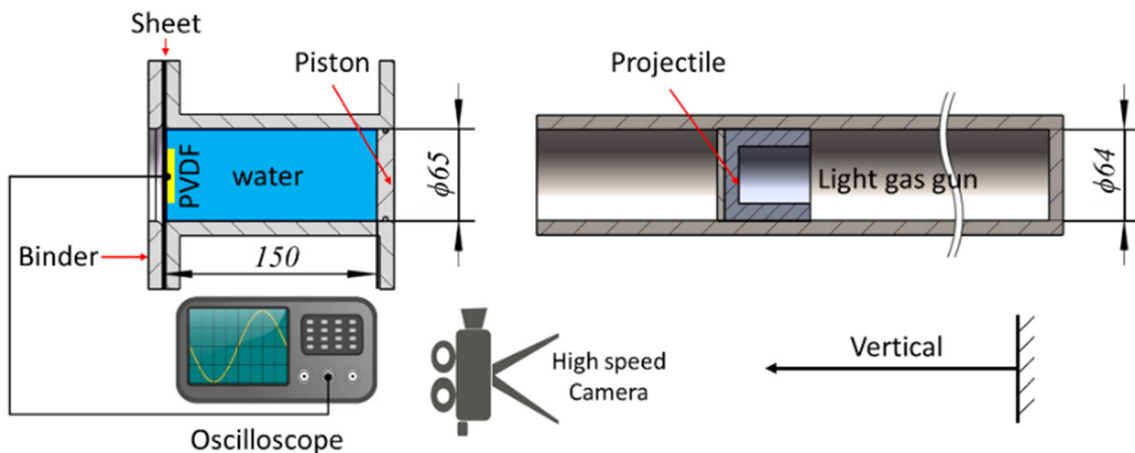


**Fig. 3** The schematic of IHF FLC test

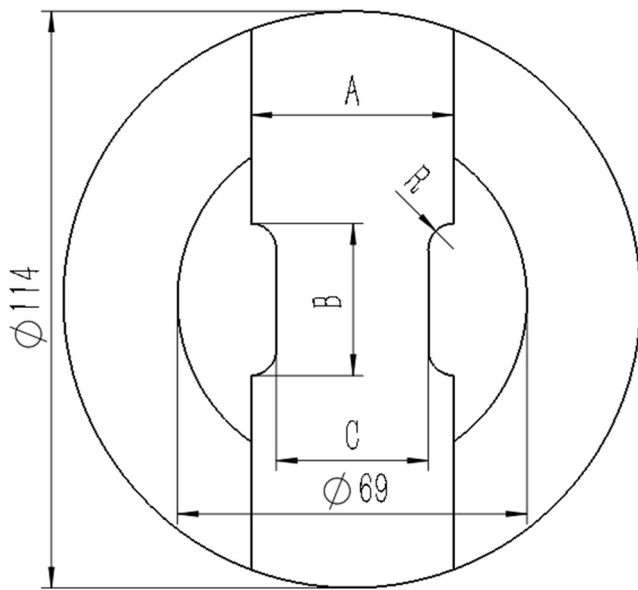


Fig. 4 The design of IHF FLC experiment specimens

using a pneumatic pressure. Accordingly, a stress wave, denoted as incident wave, is created at the incident bar and propagated to the specimen. Then, this stress wave interacts with the specimen and generates both a reflected and a transmitted stress wave. The stress wave will cause elastic strain of the bars, and the strains history produced by incident ( $\epsilon_i(t)$ ) and reflected ( $\epsilon_r(t)$ ) waves are gauged by strain gage implanted on incident bar, the strains history produced by transmitted ( $\epsilon_t(t)$ ) wave are gauged by strain gage implanted on transmitted bar, all the strain data are reported at an oscilloscope depicted in Fig. 10.

Through those reported waves, reflected and transmitted waves are used to derive and introduce the strain rates, strain and tensile stresses respectively as a function of time shown in Eq. (1) - Eq. (3). By ignoring the time terms of these parameters, the dynamic stress-strain curve is acquired for each testing condition [20].

$$\dot{\epsilon}(t) = -\frac{2c}{l_s} \epsilon_r(t) \tag{1}$$

$$\epsilon(t) = -\frac{2c}{l_s} \int_0^t \epsilon_r(t) dt = -\frac{2c}{l_s} \sum_{t=1}^n \epsilon_r(t)t \tag{2}$$

Table 2 Dimensions of IHF FLC experiment specimens and impact velocities

Dimension	1	2	3	4	5	6	7	8	9
A	20	40	40	30	50	50	50	60	whole sheet
B	50	22	30	40	12	20	24	10	
C	10	30	30	20	40	40	40	50	
R	5	5	5	5	2	5	5	2	
impact velocity (m/s)	105.8	91.7	85.2	78.6	72.1	66.4	61.5	56.2	42.3

$$\sigma(t) = -\frac{S}{S_0} E \epsilon_t(t) \tag{3}$$

Where,  $c$  is sound speed of bar.  $E$  is elastic modulus of bar.  $S$  is cross section area of bar.  $S_0$  is cross section area of specimen.  $t$  and  $t$  are time and time interval.  $\epsilon_i(t)$ ,  $\epsilon_r(t)$  and  $\epsilon_t(t)$  are incident strain, reflected strain and transmitted strain, respectively.  $l_s$  is gauge length of specimen.

The geometrical details of the tensile specimen used in HSR tensile test are shown in Fig. 11. It is more difficult to get the stable signals for sheet specimen than rod specimen in SHTB experiment. Therefore, the novel clamp is designed to prevent the sliding of the specimen and let incident stress wave transmitted to transmitted bar as much as possible.

### Theoretical calculation of FLC

Several theoretical models have been developed for the FLC calculation, M-K model is widely used in the prediction of the FLC, therefore the research will investigate the theoretical calculation of M-K model both under QS and HSR conditions, and then will compare the calculated values with experiment results. Marciniak and Kuczynski [21] proposed the model taking into account that sheet metals are non-homogeneous from both the geometrical and the structural point of view, which usually is briefly denominated as M–K model.

### Modified Johnson-Cook hardening law

The Johnson-Cook hardening law (JC) is used by considering the strain rate effect as it is widely used in the dynamic field [22].

$$\sigma = (A + B - \epsilon^n) \left( 1 + C \ln \left( \frac{\dot{\epsilon}}{\dot{\epsilon}_0} \right) \right) (1 - (T^*)^m) \tag{4}$$

where  $A$ ,  $B$ ,  $C$ ,  $n$ , and  $m$  are material constants which are experimentally determined,  $\sigma$  is the flow stress after hardening,  $\dot{\epsilon}$  is the plastic strain rate and  $\dot{\epsilon}_0$  is a user-defined reference strain rate. The strain rate of QS tensile is defined

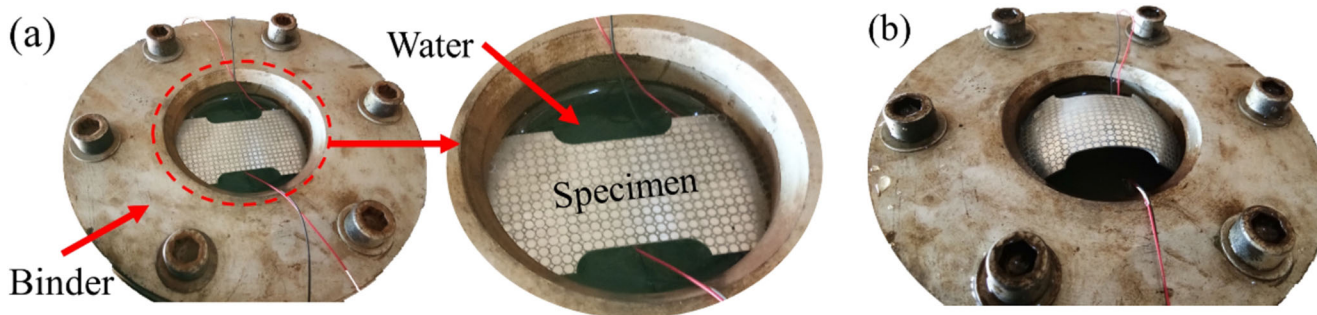


Fig. 5 Specimens (a) before, and (b) after IHF FLC test

as the reference strain rate. The  $T^*$  is defined as  $(T - T_r) / (T_m - T_r)$ ,  $T_r$  is room temperature, all the experiments are carried out under room temperature, so  $T^*$  is always equal to zero, therefore the last item of Eq. (4) can be neglected.

The stress strain curves of experiments were depicted in Fig. 12. The strain rate of the QS condition is  $10^{-3} \text{ s}^{-1}$ , and the strain rate is around  $2500 \text{ s}^{-1}$  of HSR condition which is the same to the average effective strain rate of the sheet under IHF FLC experiment. The Hopkinson tests were performed

many times until it reached a stable state, the clamping jig were improved many times for getting high quality strain wave signals, hence the measurements are reproducible. Actually, there are differences for the three high strain rate stress strain curves, the strain rate of  $2466 \text{ s}^{-1}$  and  $2488 \text{ s}^{-1}$  are similar, and the stress strain curves of these two strain rates are similar. But there is a big difference which is more than 5 % of the stress strain curve of the strain rate of  $2615 \text{ s}^{-1}$  to the stress strain curves of other two strain rates, therefore the three

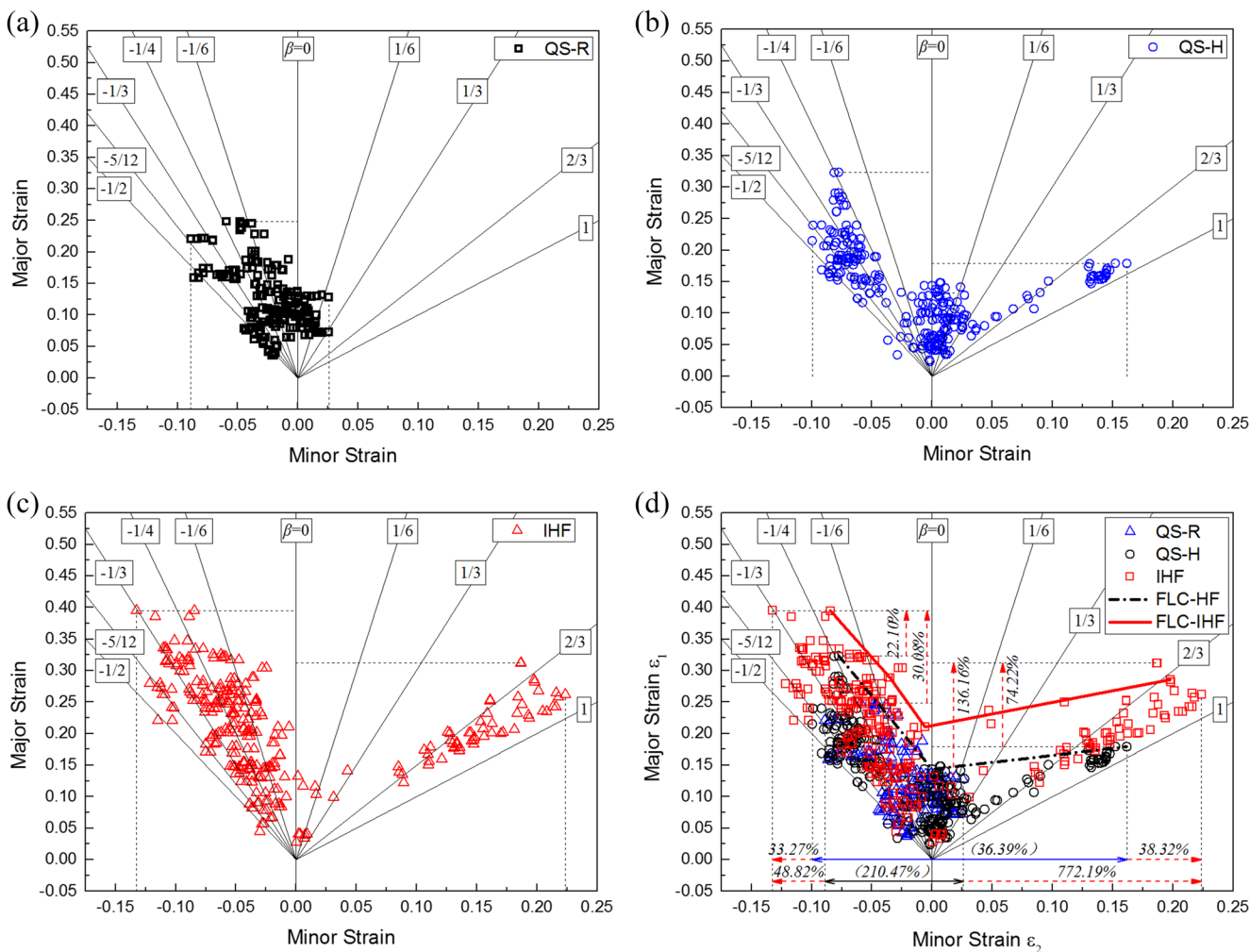


Fig. 6 FLC (a) QS-R (b) QS-H (c) IHF (d) comparisons among the three FLCs

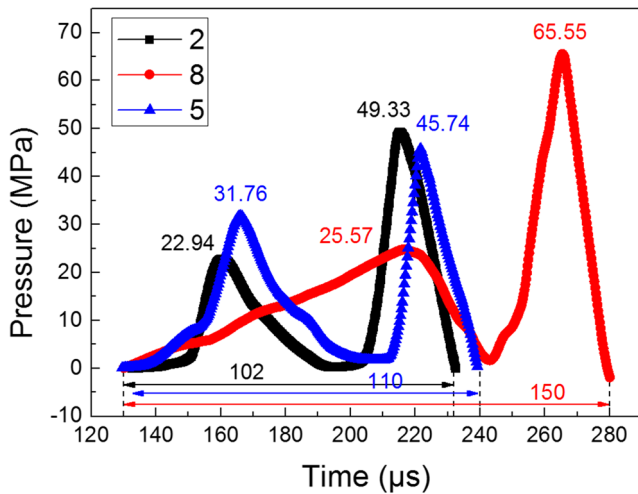


Fig. 7 Pressure wave acting on the IHF FLC experiments specimens

stress strain curves are not fully similar. The stress strain curve got from Hopkinson test is calculated from the strain wave, there will be some undulations due to the intrinsic characteristic of the test. The stress strain curve calculated from the strain waves will not be as smooth as the curve got from quasi-static tensile test.

It is found that the QS stress strain curves can be exactly fitted by Hollomon strain hardening law, therefore the first item of JC model is replaced by it, and the last item of JC is neglected due to room temperature, then the JC model transforms to Eq. (5).

$$\sigma = k - \epsilon^n \left( 1 + C \ln \left( \frac{\dot{\epsilon}}{\dot{\epsilon}_0} \right) \right) \quad (5)$$

There is a significant difference in the hardening rate between the QS load and the HSR load. Only when the plastic strain participates in the fitting, the  $n$  values corresponding to the QS and HSR conditions are 0.252 and 0.216 (Fig. 12). When Hollomon’s strain hardening law is used under both conditions, the difference between  $n$  values is 16%. It is found

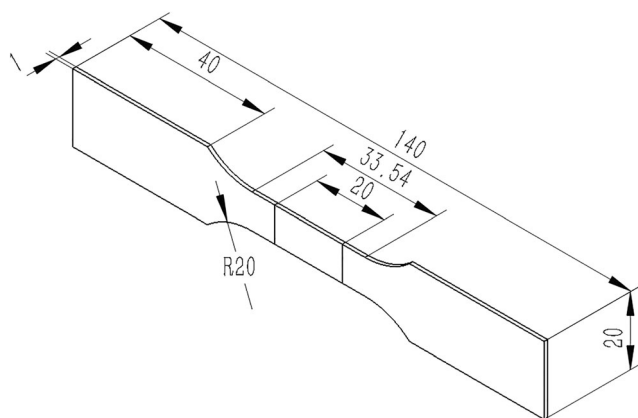


Fig. 8 Specimen used at quasi-static tensile test (all dimensions in mm)

that no matter how to adjust the strain rate hardening coefficient  $C$ , it is impossible to fit the HSR stress strain curves very well according to Eq. (5) when  $C$  is a constant as shown in Fig. 13. The  $C$  can be written as Eq. (6), and it is found that the strain rate hardening coefficient  $C$  is not a constant, it has a linear relationship with strain shown as Eq. (7), the fitting result is shown in Fig. 14. The strain-rate effect is negative when the plastic strain greater than 0.25, this demonstrates the beginning of the softening stage.

$$C(-\epsilon) = \left( \frac{\sigma_{HSR}}{\sigma_{QS}} - 1 \right) / \ln \left( \frac{\dot{\epsilon}}{\dot{\epsilon}_0} \right) \quad (6)$$

$$C(-\epsilon) = C + D - \epsilon \quad (7)$$

Therefore, a Modified Johnson-Cook hardening (MJC) law is proposed as shown in Eq. (8), it is only related to the strain under specific strain rate. For the QS condition, due to  $\dot{\epsilon} / \dot{\epsilon}_0 = 1$ , then the expression turns into the Hollomon strain-hardening law. The fitting result is shown in the Fig. 12

$$\sigma(-\epsilon) = k - \epsilon^n \left( 1 + (C + D - \epsilon) \ln \left( \frac{\dot{\epsilon}}{\dot{\epsilon}_0} \right) \right) \quad (8)$$

### Anisotropic yield criterion and anisotropic coefficients

As the anisotropic phenomena is obvious for the aluminum sheet, the Hill48 anisotropic yield criterion [23] is chosen for the calculation. The general expression of the Hill48 criterion is Eq. (9), the material is supposed to have an anisotropy with three orthogonal symmetry planes, and the shear stress is considered in the general expression of the Hill48 criterion. Moreover, the sheet is formed in a plane stress state, therefore the general expression of the Hill48 criterion will degenerate into Eq. (10) with the  $r$  value-based anisotropic coefficients.

$$2f(\sigma_{ij}) = F(\sigma_y - \sigma_z)^2 + G(\sigma_z - \sigma_x)^2 + H(\sigma_x - \sigma_y)^2 + 2L\tau_{yz}^2 + 2M\tau_{zx}^2 + 2N\tau_{xy}^2 \quad (9)$$

$$\begin{aligned} & \sigma_x^2 - \frac{2r_0}{1+r_0} \sigma_x \sigma_y + \frac{r_0+r_{90}}{r_{90}(1+r_0)} \sigma_y^2 + \frac{r_0+r_{90}}{r_{90}(1+r_0)} \\ & \times (2r_{45}+1) \tau_{xy}^2 \\ & = \sigma_0^2 \end{aligned} \quad (10)$$

Where  $\sigma_x$ ,  $\sigma_y$  and  $\tau_{xy}$  are planar components of the stress tensor,  $r_0$ ,  $r_{45}$  and  $r_{90}$  are the anisotropic coefficients of rolling direction, 45° direction and transverse direction.

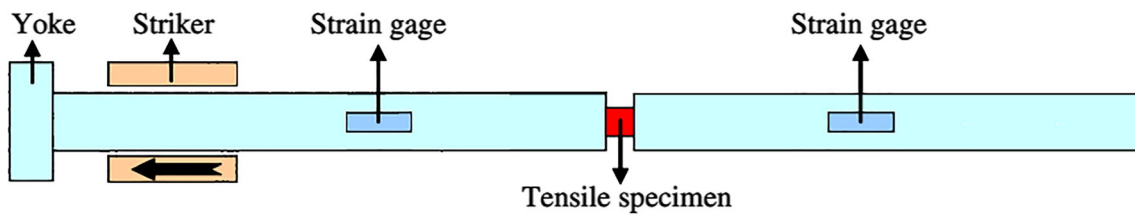
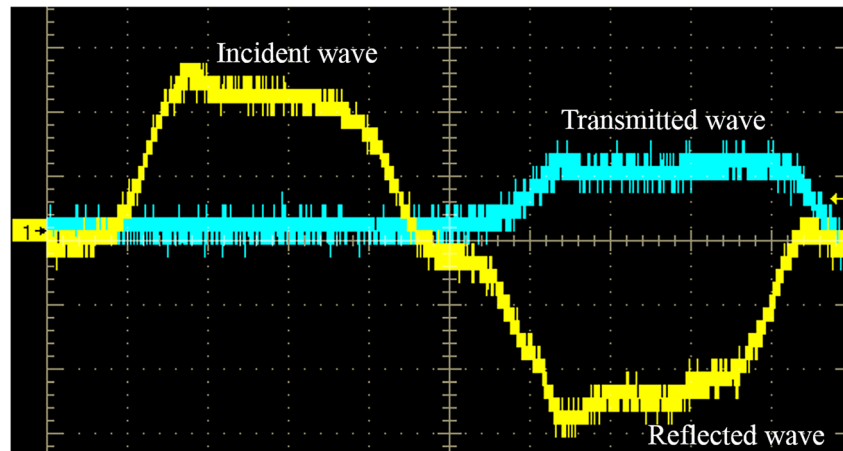


Fig. 9 The schematic of Split Hopkinson Tensile Bar (SHTB)

Fig. 10 Strain signals captured by oscilloscope



Therefore, the three parameters  $r_0, r_{45}, r_{90}$  and  $\sigma_0$  are needed to determine the yield locus. Accordingly, the tensile tests of RD, 45° and TD were accomplished under QS and HSR conditions. Afterwards, the stress strain curves of RD specimens will provide the hardening information, and the deformation of the grids of RD, 45° and TD specimens were used to calculate the anisotropic parameters.

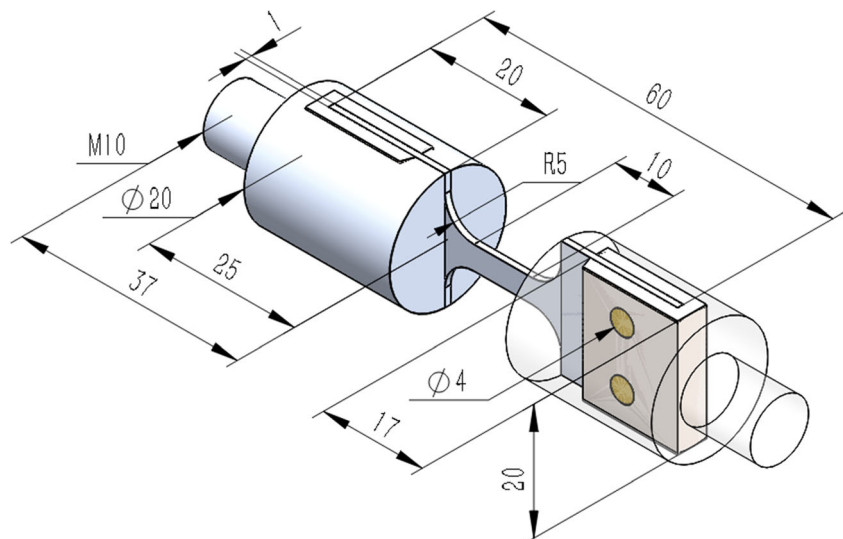
The anisotropy coefficient  $r$  is defined as the ratio of width strain and thickness strain. As the thickness of the specimen is obviously (usually by at least one order) small compared to its width, the relative errors of measurement of the two strains

will be quite distinct. Therefore the above relationships are replaced by the relationship of longitudinal strain and width strain of the specimen. Taking into account the condition of volume constancy, the following form of  $r$  is obtained.

$$r = \frac{\varepsilon_2}{\varepsilon_3} = -\frac{\varepsilon_2}{\varepsilon_1 + \varepsilon_2} \quad (11)$$

The shape of grids gradually changes during the uniaxial tensile test as shown in Fig. 15. The diameter of circle grids of QS and HSR are 1 mm and 0.5 mm respectively. The grids pattern are aligned along the uniaxial tension direction.

Fig. 11 Schematic of novel clamp and specimen used in SHTB (all dimensions in mm)





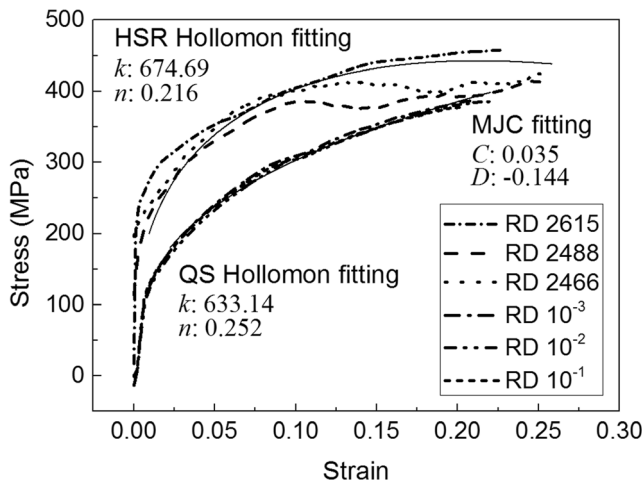


Fig. 12 Stress-strain curves under QS and HSR conditions

It is found that the  $r$  value is different from grid to grid in the same specimen, usually the  $r$  value is directly calculated by the data acquired by extensometer, but it is an average result of the whole gauge length. Therefore, the statistical method is adopted to calculate the  $r$  value more accurately according to Kim et al. [24]. The longitudinal strain and the width strain of the grids in the gauge length were plotted as a point in a coordinate system (Fig. 16). The longitudinal strain and the width strain from 0 to fracture location are considered, therefore, it can fully reflect the change of the  $r$  coefficients along the uniaxial tensile direction. A linear fitting is setup by the least squares method, the slope  $k$  of the line is the accurate value of  $\varepsilon_2/\varepsilon_1$ , substitute the  $k$  into Eq. (11), then the  $r$  value can be calculated by the Eq. (12). It is found that the  $r$  values distributed more dispersed from the rolling direction to the transverse direction, which is maybe related to the texture characteristic caused by the rolling process producing the sheet. Furthermore, the  $r$  values distribution of HSR is more dispersed than QS. This further demonstrates that the average

$r$  value calculated by using extensometers does not fully reflect the anisotropic characteristic of the material. The RD anisotropic coefficients are 0.563 and 0.865 under QS and HSR conditions, respectively, the 45° ones are 1.268 and 0.801 under the two conditions, the TD ones are 0.923 and 0.491 under the two conditions.

$$r = -\frac{k}{1+k} \tag{12}$$

**FLCs of theoretical calculation**

The M-K theory is calculated according to Ganjiani and Assempour [25]. There are several researches investigated the modelling of FLCs under dynamic loading conditions [26–28], and it is found that the initial thickness ratio shows a major effect to the M-K calculation results. Whereas, all these works only investigated the biaxial strain state, and didn't include the tension-compression strain state. Meanwhile, it is found that inertia induced postpone the necking during dynamic loading, making a notable contribution to the formability improvement of materials at high strain rates [29–31]. In addition, the initial thickness ratio  $f$  represents the geometrical or microstructural inhomogeneous of materials, and greatly affect the formability controlled by necking process. To consider the necking postpone effect of the inertia, a larger value of  $f$  can be assigned for the IHF forming with high strain rate which means a decreasing of materials inhomogeneity. Therefore, the initial thickness ratio is set to be 0.95 and 0.992 for QS and HSR conditions, respectively. The increment of the major principal strain of perfect zone A is set to  $1 \times 10^{-6}$ .

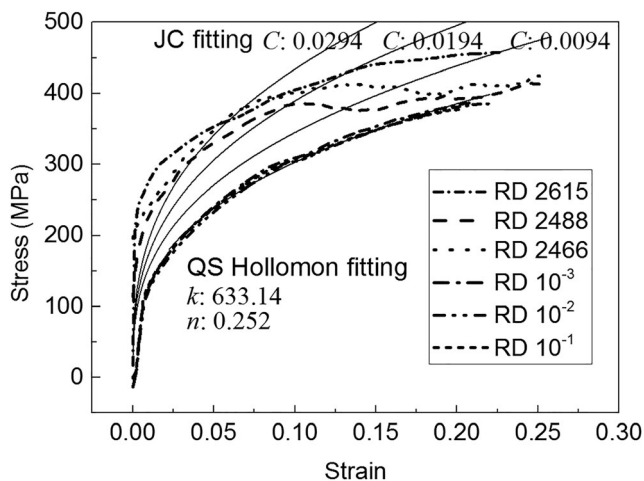


Fig. 13 Fitting results of original JC

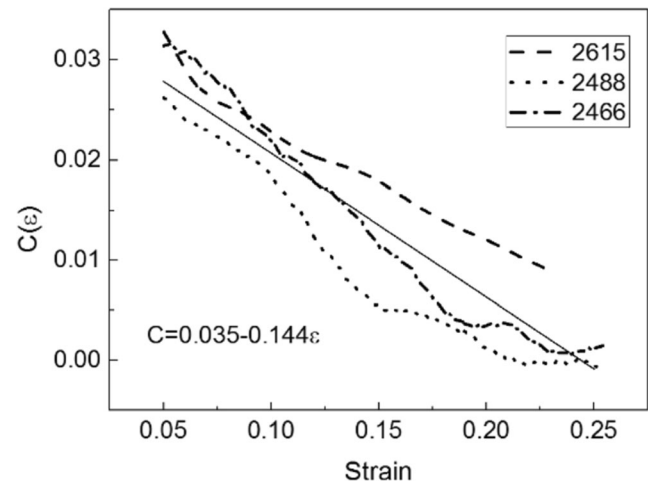
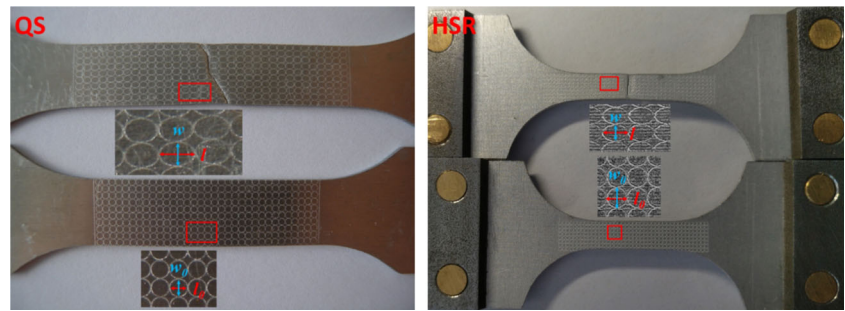


Fig. 14 The relationship of  $C$  and strain

**Fig. 15** The calculation of the anisotropic coefficient



The theoretical calculation of the FLCs will combine the Hollomon hardening law and anisotropic yield criterion. The Hollomon strain hardening law will provide the  $n$  values of QS and HSR conditions which are depicted in Fig. 12. The HSR strain hardening value  $n$  is smaller than the one of QS, the calculated FLC under HSR condition will be lower than the one under QS condition if the same  $f$  value is used (Fig. 17a). This result is attributed to that

the calculated value of the FLC is highly depended on the strain hardening coefficient  $n$ , the value of  $n$  is larger, the FLC is higher, and the value of  $n$  is smaller, and the FLC is lower. Therefore the calculated FLC under HSR condition are lower than that under QS condition based on the same  $f$  value, but this calculation results are not in agreement with the experimental results. The calculation FLC of HSR condition is higher than the one of QS condition

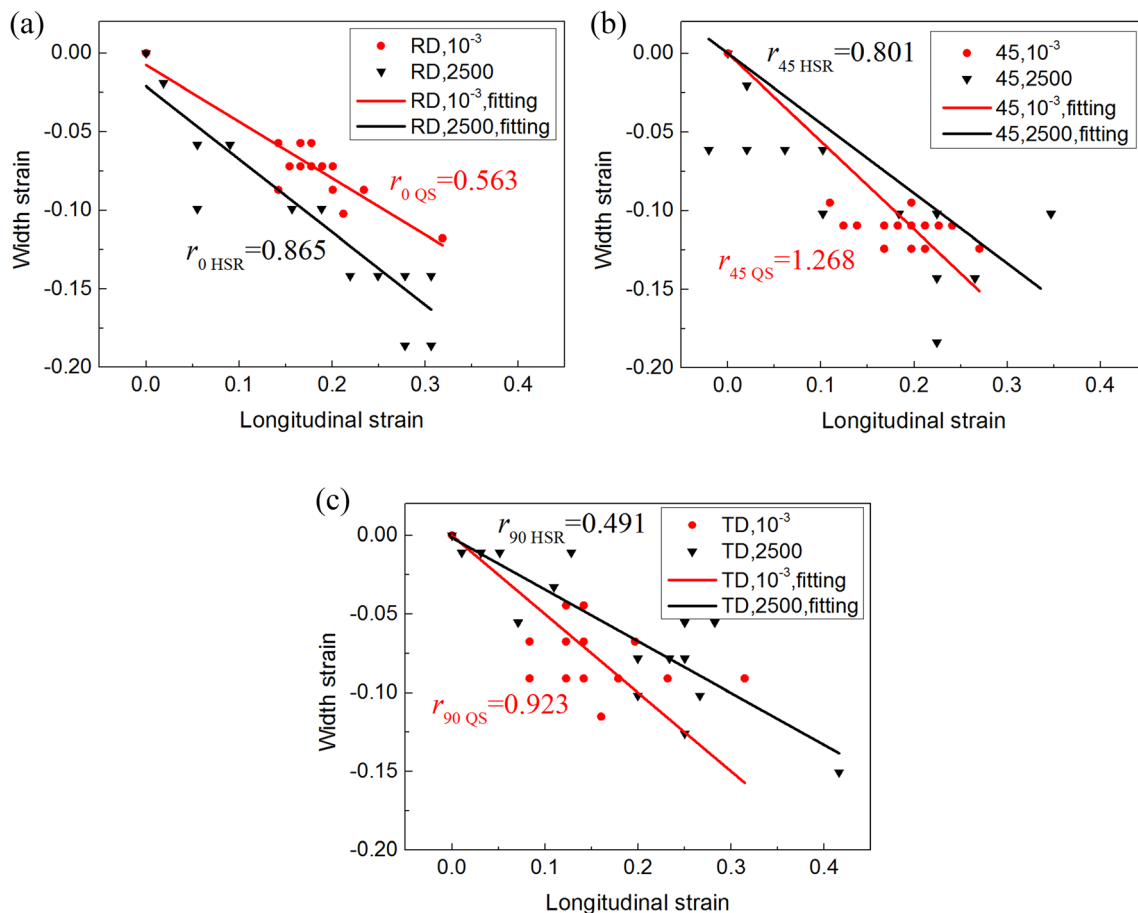


**Fig. 16** The anisotropic coefficients under QS and HSR conditions (a) RD (b) 45° (c) TD

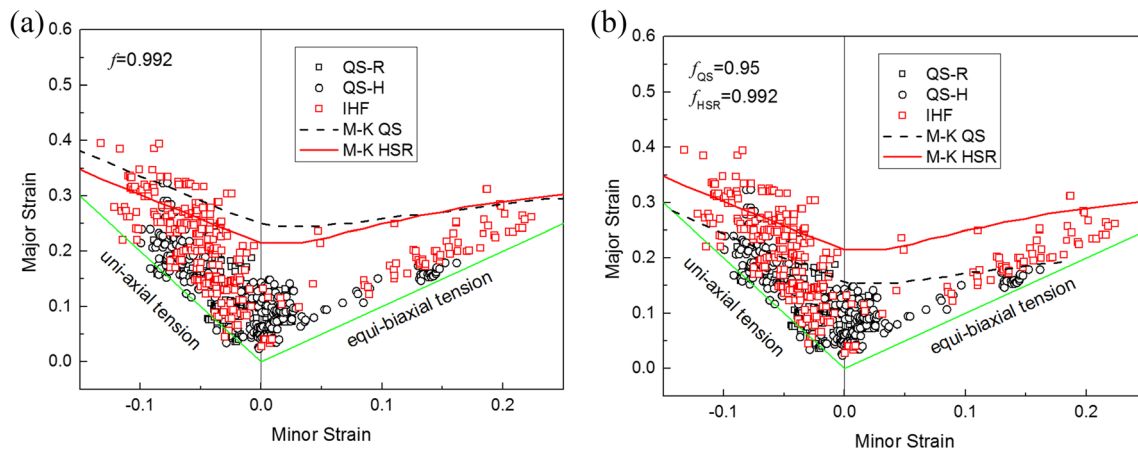


**Fig. 17** Calculated FLCs by M-K theory under QS and HSR conditions.

by using different  $f$  value (Fig. 17b), and it is found that the FLCs calculated by M-K theory are close to the experimental values under QS and HSR conditions. It is proved that the HSR FLC is able to be calculated by the traditional theory according to some HSR tensile tests which are easier than the complicated IHF FLC experiments.

## Conclusions

The frictionless full zone hydraulic FLC can be realized by IHF without the carrier sheet for tension-compression zone. It is concluded that the formability of aluminum sheet under impact hydroforming can be potentially improved at room temperature. The range of minor strain of IHF FLC increases 210.47 and 36.39 % compared with the FLCs of QS-R and QS-H for the whole FLC zone. The increase of the biaxial tension zone is much more than the increase of the tension-compression zone for IHF FLC compared with the QS-H FLC. The strain rate of IHF is able to reach  $2.43 \times 10^3 \text{ s}^{-1}$ . The M-K model combined with the Hollomon hardening law and the Hill48 anisotropic yield criterion can be used to calculate the FLC of the sheet under HSR condition with a larger initial thickness ratio by considering the neck postponing effect of inertia. The results calculated by the M-K model are in a good agreement with those obtained from experimentation which implies that the traditional theory is able to predict the FLC under HSR conditions.

**Supplementary Information** The online version contains supplementary material available at <https://doi.org/10.1007/s12289-021-01635-7>.

**Abbreviations** QS, quasi-static; HSR, high strain rate; FLC, forming

(a) the same  $f$  value (b) different  $f$  values

limit curve; QS-R, quasi-static rigid punch; QS-H, quasi-static hydraulic punch; HF, hydroforming; IHF, impact hydroforming; M-K, Marciniak and Kuczynski model; SHTB, Split Hopkinson Tensile Bar test; SHPB, Split Hopkinson Pressure Bar test; RD, rolling direction; TD, transverse direction

## Declarations

**Conflict of interests** The authors declare that they have no conflict of interest.

## References

- Zhang SH (1999) Developments in hydroforming. *J Mater Proc Technol* 91:236–244
- Zhang SH (2004) Recent developments in sheet hydroforming technology. *J Mater Proc Technol* 151:237–241
- Suttner S, Merklein M (2016) Experimental and numerical investigation of a strain rate controlled hydraulic bulge test of sheet metal. *J Mater Proc Technol* 235:121–133
- Lee JY, Xu L, Barlat F, Wagoner RH, Lee MG (2013) Balanced biaxial testing of advanced high strength steels in warm conditions. *Exp Mech* 53:1681–1692
- Grolleau V, Gary G, Mohr D (2008) Biaxial testing of sheet materials at high strain rates using viscoelastic bars. *Exp Mech* 48:293–306
- Banabic D, Lazarescu L, Paraianu L, Ciobanu I, Nicodim I, Comsa DS (2013) Development of a new procedure for the experimental determination of the Forming Limit Curves. *CIRP Ann* 62:255–258
- Chen YY, Tsai YC, Huang CH (2014) Integrated Hydraulic bulge and forming limit testing method and apparatus for sheet metals. *Key Eng Mater* 626:171–177
- Zhang L, Min JY, Carsley JE, Stoughton TB, Lin JP (2017) Experimental and theoretical investigation on the role of friction in Nakazima testing. *Int J Mech Sci* 133:217–226
- Ma Y, Xu Y, Zhang SH, Banabic D, El-Aty A, Chen A, Chen DY (2018) Investigation on formability enhancement of 5A06 aluminum sheet by impact hydroforming. *CIRP Ann* 67:281–284

10. Broomhead P, Grieve RJ (1982) The effect of strain rate on the strain to fracture of a sheet steel under biaxial tensile stress conditions. *J Eng Mater Technol* 104:102–106
11. Ramezani M, Ripin ZM (2010) Combined experimental and numerical analysis of bulge test at high strain rates using split Hopkinson pressure bar apparatus. *J Mater Process Technol* 210:1061–1069
12. Justusson B, Pankow M, Heinrich C, Rudolph M, Waas AM (2013) Use of a shock tube to determine the bi-axial yield of an aluminum alloy under high rates. *Int J Impact Eng* 58:55–65
13. Golovashchenko SF (2007) Material formability and coil design in electromagnetic forming. *J Mater Eng Perform* 16:314–320
14. Yu H, Zheng Q (2019) Forming limit diagram of DP600 steel sheets during electrohydraulic forming. *Int J Adv Manuf Technol* 104:743–756
15. Verleysen P, Peirs J, Van Slycken J, Faes K, Duchene L (2011) Effect of strain rate on the forming behaviour of sheet metals. *J Mater Process Technol* 211:1457–1464
16. Chuang KC, Ma CC, Chang CK (2014) Determination of dynamic history of impact loadings using polyvinylidene fluoride (pvdf) films. *Exp Mech* 54:483–488
17. Bauer F (2004) PVDF shock compression sensors in shock wave physics. *AIP Conf Proc* 706:1121–1124
18. Maris C, Hassannejadasl A, Green DE (2016) Comparison of quasi-static and electrohydraulic free forming limits for DP600 and AA5182 sheets. *J Mater Process Technol* 235:206–219
19. El-Magd E, Abouridouane M (2006) Characterization, modelling and simulation of deformation and fracture behaviour of the light-weight wrought alloys under high strain rate loading. *Int J Impact Eng* 32:741–758
20. Mirone G, Corallo D, Barbagallo R (2017) Experimental issues in tensile Hopkinson bar testing and a model of dynamic hardening. *Int J Impact Eng* 103:180–194
21. Marciniak Z, Kuczynski K (1967) Limit strains in the process of stretch-forming sheet metal. *Int J Mech Sci* 9:609–620
22. Johnson GR, Cook WH (1983) A constitutive model and data for metals subjected to large strains, high strain rates and high temperatures. *Proceedings of the 7th International Symposium on Ballistics*, pp 541–547
23. Hill R (1948) A theory of the yielding and plastic flow of anisotropic metals. *Proc Roy Soc Lond A* 193:281–297
24. Kim SB, Huh H, Bok HH, Moon MB (2011) Forming limit diagram of auto-body steel sheets for high-speed sheet metal forming. *J Mater Process Technol* 211:851–862
25. Ganjiani M, Assempour A (2007) An improved analytical approach for determination of forming limit diagrams considering the effects of yield functions. *J Mater Process Technol* 182:598–607
26. Zaera R, Rodríguez-Martínez JA, Vadillo G, Fernández-Sáez J, Molinari A (2015) Collective behaviour and spacing of necks in ductile plates subjected to dynamic biaxial loading. *J Mech Phys Solids* 85:245–269
27. Jacques N (2020) An analytical model for necking strains in stretched plates under dynamic biaxial loading. *Int J Solids Struct* 200:198–212
28. N'souglo KE, Jacques N, Rodríguez-Martínez JA (2021) A three-pronged approach to predict the effect of plastic orthotropy on the formability of thin sheets subjected to dynamic biaxial stretching. *J Mech Phys Solids* 146:104189
29. Xue Z, Vaziri A, Hutchinson JW (2008) Material aspects of dynamic neck retardation. *J Mech Phys Solids* 56:93–113
30. Ghosh AK (1977) The influence of strain hardening and strain-rate sensitivity on sheet metal forming. *J Eng Mater Technol* 99:264–274
31. Hutchinson JW, Neale KW (1977) Influence of strain-rate sensitivity on necking under uniaxial tension. *Acta Metall* 25:839–846

**Publisher's Note** Springer Nature remains neutral with regard to jurisdictional claims in published maps and institutional affiliations.